Research Article | Vol. 24, No. 22 | 31 Oct 2016 | OPTICS EXPRESS 24824
Optics EXPRESS

Anomalous circular dichroism in high harmonic generation of stereoisomers with two chiral centers

XIAOSONG ZHU,[1] XI LIU,[1] PENGFEI LAN,[1,3] DIAN WANG,[1] QINGBIN ZHANG,[1] WEI LI,[1] AND PEIXIANG LU[1,2,*]

[1]*Wuhan National Laboratory for Optoelectronics and School of Physics, Huazhong University of Science and Technology, Wuhan 430074, China*
[2]*Laboratory of Optical Information Technology, Wuhan Institute of Technology, Wuhan 430205, China*
[3]*pengfeilan@mail.hust.edu.cn*
[*]*lupeixiang@mail.hust.edu.cn*

Abstract: When a molecule has more than one chiral center, it can be either a chiral molecule or a meso isomer. High harmonic generation (HHG) of stereoisomers with two chiral centers driven by circularly polarized (CP) laser pulses is investigated. Counterintuitively, it is found that the HHG exhibits prominent circular dichroism for the meso isomer, while the harmonic spectra with left and right CP laser pulses are nearly the same for the chiral isomers. We show that the anomalous circular dichroism is attributed to the characteristic recollision dynamics of HHG. This feature makes the HHG a promising tool to discriminate the meso isomer and racemic mixture, where no optical activity can be found in both cases. Similar dichroism responses are also found by applying the counter-rotating bicircular laser pulses.

OCIS codes: (190.4160) Multiharmonic generation; (270.6620) Strong-field processes; (160.1585) Chiral media.

References and links

1. U. J. Meierhenrich, *Amino acids and the Asymmetry of Life* (Springer, 2008).
2. H. Tsukube, and S. Shinoda, "Lanthanide Complexes in Molecular Recognition and Chirality Sensing of Biological Substrates," Chem. Rev. **102**, 2389–2403 (2002).
3. T. Eriksson, S. Björkman, B. Roth, Å Fyge, and P. Höglund, "Ctereospecific determination, chiral inversion in vitro and pharmacokinetics in humans of the enantiomers of thalidomide," Chirality **7**, 44–52 (1995).
4. G. D. Fasman, *Circular Dichroism and the Conformational Analysis of Biomolecules* (Springer, 1996).
5. I. Tinoco, and D. H. Turner, "Fluorescence detected circular dichroism. Theory," J. Opt. Soc. Am. B **98**, 6453–6456 (1976).
6. I. Powis, "Photoelectron circular dichroism in chiral molecules," Adv. Chem. Phys. **138**, 267–329 (2008).
7. X. Zhu, P. Lan, K. Liu, Y. Li, X. Liu, Q. Zhang, I. Barth, and P. Lu, "Helicity sensitive enhancement of strong-field ionization in circularly polarized laser fields," Opt. Express **24**, 4196–4209 (2016).
8. D. Patterson, M. Schnell, and J. M. Doyle, "Enantiomer-specific detection of chiral molecules via microwave spectroscopy," Nature **497**, 475–477 (2013).
9. A. Yachmenev, and S. N. Yurchenko, "Detecting chirality in molecules by linearly polarized laser fields," Phys. Rev. Lett. **117**, 033001 (2016).
10. L. Nahon, G. A. Garcia, C. J. Harding, E. Mikajlo, and I. Powis, "Determination of chiral asymmetries in the valence photoionization of camphor enantiomers by photoelectron imaging using tunable circularly polarized light," J. Chem. Phys. **125**, 114309 (2006).
11. C. Lux, M. Wollenhaupt, T. Bolze, Q. Liang, J. Kohler, C. Sarpe, and T. Baumert, "Circular dichroism in the photoelectron angular distributions of camphor and fenchone from multiphoton ionization with femtosecond laser pulses," Angew. Chem. Int. Ed. **51**, 5001–5005 (2012).
12. I. Dreissigacker, and M. Lein, "Photoelectron circular dichroism of chiral molecules studied with a continuum-state-corrected strong-field approximation," Phys. Rev. A **89**, 053406 (2014).
13. R. Cireasa, A. E. Boguslavskiy, B. Pons, M. C. H. Wong, D. Descamps, S. Petit, H. Ruf, N. Thiré, A. Ferré, J. Suarez, J. Higuet, B. E. Schmidt, A. F. Alharbi, F. Légaré, V. Blanchet, B. Fabre, S. Patchkovskii, O. Smirnova, Y. Mairesse, and V. R. Bhardwaj, "Probing molecular chirality on a sub-femtosecond timescale," Nat. Phys. **11**, 654–658 (2015).
14. O. Smirnova, Y. Mairesse, and S. Patchkovskii, "Opportunities for chiral discrimination using high harmonic generation in tailored laser fields," J. Phys. B: At. Mol. Opt. Phys. **48**, 234005 (2015).

#273980 http://dx.doi.org/10.1364/OE.24.024824
Journal © 2016 Received 16 Aug 2016; revised 12 Oct 2016; accepted 13 Oct 2016; published 17 Oct 2016

Optics EXPRESS

15. L. He, P. Lan, Q. Zhang, C. Zhai, F. Wang, W. Shi, and P. Lu, "Spectrally resolved spatiotemporal features of quantum paths in high-order-harmonic generation," Phys. Rev. A **92**, 043403 (2015).
16. O. Kfir, P. Grychtol, E. Turgut, R. Knut, D. Zusin, D. Popmintchev, T. Popmintchev, H. Nembach, J. M. Shaw, A. Fleischer, H. Kapteyn, M. Murnane, and O. Cohen, "Generation of bright phase-matched circularly-polarized extreme ultraviolet high harmonics," Nat. Photonics **9**, 99–105 (2014).
17. P. B. Corkum, "Plasma perspective on strong field multiphoton ionization," Phys. Rev. Lett. **71**, 1994–1997 (1993).
18. K. Schafer, B. Yang, L. DiMauro, and K. Kulander, "Above threshold ionization beyond the high harmonic cutoff," Phys. Rev. Lett. **70**, 1599–1602 (1993).
19. X. Zhu, X. Liu, Y. Li, M. Qin, Q. Zhang, P. Lan, and P. Lu, "Molecular high-order-harmonic generation due to the recollision mechanism by a circularly polarized laser pulse," Phys. Rev. A **91**, 043418 (2015).
20. K. Hoki, D. Kröner, J. Manz, "Selective preparation of enantiomers from a racemate by laser pulses: model simulation for oriented atropisomers with coupled rotations and torsions," Chem. Phys. **267**, 59–79 (2001).
21. S. Kodama, A. Yamamoto, A. Matsunaga, K. Hayakawa, "Direct chiral resolution of tartaric acid in food products by ligand exchange capillary electrophoresis using copper(II)-D-quinic acid as a chiral selector," J. Chromatogr. A **932**, 139–143 (2001).
22. E. Runge, and E. K. U. Gross, "Density-functional theory for time-dependent systems," Phys. Rev. Lett. **52**, 997–1000 (1984).
23. J. P. Perdew, and A. Zunger, "Self-interaction correction to density-functional approximations for many-electron systems," Phys. Rev. B **23**, 5048–5079 (1981).
24. N. Troullier and J. L. Martins, "Efficient pseudopotentials for plane-wave calculations," Phys. Rev. B **43**, 1993 (1991).
25. M. A. L. Marques, A. Castro, G. F. Bertsch, and A. Rubio, "Octopus: a first-principles tool for excited electron-ion dynamics," Comput. Phys. Commun. **151**, 60–78 (2003).
26. A. Castro, H. Appel, Micael Oliveira, C. A. Rozzi, X. Andrade, F. Lorenzen, M. A. L. Marques, E. K. U. Gross, and A. Rubio, "Octopus: a tool for the application of time-dependent density functional theory," Phys. Stat. Sol. B **243**, 2465–2488 (2006).
27. X. Andrade, D. A. Strubbe, U. De Giovannini, A. H. Larsen, M. J. T. Oliveira, J. Alberdi-Rodriguez, A. Varas, I. Theophilou, N. Helbig, M. Verstraete, L. Stella, F. Nogueira, A. Aspuru-Guzik, A. Castro, M. A. L. Marques, and A. Rubio, "Real-space grids and the Octopus code as tools for the development of new simulation approaches for electronic systems," Phys. Chem. Chem. Phys. **17**, 31371–31396 (2015).
28. Gaussian 09, Revision D.01, M. J. Frisch, G. W. Trucks, H. B. Schlegel, G. E. Scuseria, M. A. Robb, J. R. Cheeseman, G. Scalmani, V. Barone, B. Mennucci, G. A. Petersson, H. Nakatsuji, M. Caricato, X. Li, H. P. Hratchian, A. F. Izmaylov, J. Bloino, G. Zheng, J. L. Sonnenberg, M. Hada, M. Ehara, K. Toyota, R. Fukuda, J. Hasegawa, M. Ishida, T. Nakajima, Y. Honda, O. Kitao, H. Nakai, T. Vreven, J. A. Montgomery, Jr., J. E. Peralta, F. Ogliaro, M. Bearpark, J. J. Heyd, E. Brothers, K. N. Kudin, V. N. Staroverov, R. Kobayashi, J. Normand, K. Raghavachari, A. Rendell, J. C. Burant, S. S. Iyengar, J. Tomasi, M. Cossi, N. Rega, J. M. Millam, M. Klene, J. E. Knox, J. B. Cross, V. Bakken, C. Adamo, J. Jaramillo, R. Gomperts, R. E. Stratmann, O. Yazyev, A. J. Austin, R. Cammi, C. Pomelli, J. W. Ochterski, R. L. Martin, K. Morokuma, V. G. Zakrzewski, G. A. Voth, P. Salvador, J. J. Dannenberg, S. Dapprich, A. D. Daniels, Ö. Farkas, J. B. Foresman, J. V. Ortiz, J. Cioslowski, and D. J. Fox, Gaussian, Inc., Wallingford CT, 2009.
29. J. Hansen, H. Stapelfeldt, D. Dimitrovski, M. Abu-samha, C. Martiny, and L. Madsen, "Time-resolved photoelectron angular distributions from strong-field ionization of rotating naphthalene molecules," Phys. Rev. Lett. **106**, 073001 (2011).
30. J. L. Hansen, J. H. Nielsen, C. B. Madsen, A. T. Lindhardt, M. P. Johansson, T. Skrydstrup, L. B. Madsen, and H. Stapelfeldt, "Control and femtosecond time-resolved imaging of torsion in a chiral molecule," J. Chem. Phys. **136**, 204310 (2012).
31. M. Li, P. Zhang, S. Luo, Y. Zhou, Q. Zhang, P. Lan, and P. Lu, "Selective enhancement of resonant multiphoton ionization with strong laser fields," Phys. Rev. A **92**, 063404 (2015).
32. F. Mauger, A. D. Bandrauk, and T. Uzer, "Circularly polarized molecular high harmonic generation using a bicircular laser," J. Phys. B: At. Mol. Opt. Phys. **49**, 10LT01 (2016).
33. X. Liu, X. Zhu, L. Li, Y. Li, Q. Zhang, P. Lan, P. Lu, "The selection rules of high harmonic generation: roles of projections of molecules and dynamical directivities of laser fields," Phys. Rev. A **94**, 033410 (2016).
34. M. Ivanov, T. Brabec, and N. Burnett, "Coulomb corrections and polarization effects in high-intensity high-harmonic emission," Phys. Rev. A **54**, 742 (1996).
35. X. Zhu, M. Qin, Q. Zhang, Y. Li, Z. Xu, and P. Lu, "Influence of large permanent dipoles on molecular orbital tomography," Opt. Express **21**, 5255–5268 (2013).
36. C. Chirilă, "Analysis of the strong field approximation for harmonic generation and multiphoton ionization in intense ultrashort laser pulses," Ph.D. thesis, University of Durham, 2004.
37. D. B. Milošević, W. Becker, and R. Kopold, "Generation of circularly polarized high-order harmonics by two-color coplanar field mixing", Phys. Rev. A **61**, 063403 (2000).
38. D. B. Milošević, "Circularly polarized high harmonics generated by a bicircular field from inert atomic gases in the p state: A tool for exploring chirality-sensitive processes," Phys. Rev. A **92**, 043827 (2015).
39. D. B. Milošević, "High-order harmonic generation by a bichromatic elliptically polarized field: conservation of

Optics EXPRESS

angular momentum," J. Phys. B: At. Mol. Opt. Phys. **48**, 171001 (2015).
40. T. T. Luu, M. Garg, S. Y. Kruchinin, A. Moulet, M. T. Hassan, and E. Goulielmakis, "Extreme ultraviolet high-harmonic spectroscopy of solids," Nature **521**, 498–502 (2015).
41. G. Ndabashimiye, S. Ghimire, M. Wu, D. A. Browne, K. J. Schafer, M. B. Gaarde, and D. A. Reis, "Solid-state harmonics beyond the atomic limit," Nature **534**, 520–523 (2016).

1. Introduction

A chiral center is a stereocenter consisting of an atom holding a set of ligands (atoms or groups of atoms) in a spatial arrangement which is not superimposable on its mirror image. If a molecule has a chiral center, it is a chiral molecule and has a non-superposable mirror image which is also chiral (known as an enantiomer). The property of chirality is of great practical importance because most biomolecules and pharmaceuticals are chiral and many chemical processes in living beings are chirality dependent [1]. Therefore, detection and recognition of chirality is one of the most important and challenging tasks for researches and applications in the biological and pharmaceutical areas [2, 3].

The basic idea to detect the chirality is to utilize the different responses of the target to left and right circularly polarized (CP) light [4–7] or to other forms of light [8, 9]. With the fast development of laser techniques, several novel methods for chirality detection in the gas phase using femtosecond laser pulses were proposed and implemented. For example, in the spirit of photoelectron circular dichroism (PECD) [6, 10], the chirality can be recognized from the asymmetric photoelectron angular distribution based on the strong-field ionization driven by CP femtosecond laser pulses [11, 12]. With this method, the circular dichroism (CD) signal up to 10% was obtained, and the CD can be even higher if the molecule is oriented. In a recent work, it is shown that the chirality can be detected with the high harmonic generation (HHG) [13, 14]. The HHG is a strong-field process when molecules are irradiated by femtoseond laser pulses [15, 16] and can be understood with the semiclassical three-step recollision model [17–19]. The chiral HHG method has several advantages compared with conventional CD techniques, such as the high magnitude of CD signal, the capability of resolving the chiral dynamics on the sub-femtosecond timescale, etc.

Up to now, only molecules with one chiral center have been considered for the strong-field chirality detection techniques. A molecule can have more than one chiral center. In this case, the molecule can be either chiral or achiral. For example, if a molecule has two R-type (S-type) chiral centers, it is a right-handed (left-handed) chiral molecule. However, if the molecule has two enantiomeric chiral centers which are R-type and S-type respectively, it is an achiral molecule known as a meso isomer. Since a meso isomer has different properties compared with its chiral isomers in chirality dependent processes, it is also demanding to recognize and purify/eliminate meso isomer for biological and pharmaceutical researches and applications [20, 21]. However, as both the meso isomer and the racemic mixture (the mixture that has equal amounts of left- and right-handed enantiomers) do not present optical activity, it is difficult to discriminate the meso and racemic samples with conventional CD techniques.

In this work, we investigate the HHG of molecules with two chiral centers driven by CP laser pulses. Due to the characteristic recollision dynamics in HHG, anomalous CD is found: the obtained harmonic spectra with left and right CP laser pulses are different for the meso isomer, while the spectra are nearly the same for its chiral isomers. This feature promises that the HHG can be an efficient tool to discriminate the meso isomer and racemic mixture. Furthermore, similar dichroism responses are also found in HHG driven by counter-rotating bicircular (CRB) laser pulses.

Optics EXPRESS

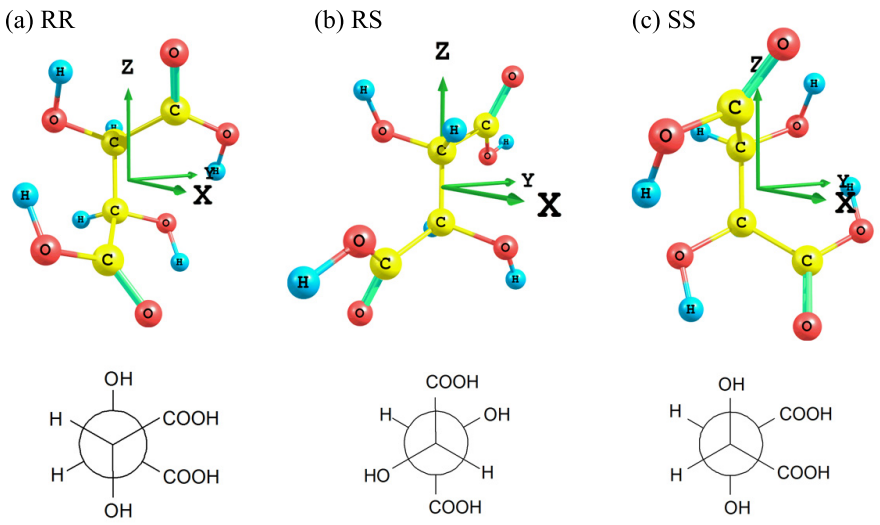

Fig. 1. Structures of the three stereoisomers of tartaric acid. Panel (a) shows the right-handed chiral isomer with two R-type chiral carbons, which is denoted as the RR-tartaric acid. Panel (b) shows the meso isomer with one R-tpye chiral carbon in the upper half and one S-type chiral carbon in the lower half, which is denoted as the RS-tartaric acid. Panel (c) shows the left-handed chiral isomer with two S-type chiral carbons, which is denoted as the SS-tartaric acid. The Newman projections of the molecules are presented below the structures, respectively.

2. Theoretical model

The HHG process of molecules in response to laser fields are simulated by using the three-dimensional time-dependent density-functional theory (TDDFT) [22]. The evolutions of the systems follow the time-dependent Kohn-Sham (TDKS) equations (atomic units are used unless otherwise stated)

$$i\frac{\partial}{\partial t}\Psi_i(\mathbf{r},t) = [-\frac{\nabla^2}{2} + v_s(\mathbf{r},t)]\Psi_i(\mathbf{r},t), \quad i = 1,2,\cdots,N. \tag{1}$$

N is the number of Kohn-Sham (KS) orbitals $\Psi_i(\mathbf{r},t)$. In the simulation, only the electrons in the valence shell are active, and we neglect electron spin effects. $v_s(\mathbf{r},t)$ is the KS potential defined as

$$v_s(\mathbf{r},t) = \int \frac{\rho(\mathbf{r}',t)}{|\mathbf{r}-\mathbf{r}'|}d\mathbf{r}' + v_{xc}(\mathbf{r},t) + v_{ne} + v_{las}. \tag{2}$$

$\rho(\mathbf{r},t)$ is the time-dependent density of the multi-electron interacting system given by $\rho(\mathbf{r},t) = \sum_{i=1}^{N}|\Psi_i(\mathbf{r},t)|^2$. v_{xc} is the exchange-correlation potential including all non-trivial many body effects. Here, we apply the local-density approximation (LDA) incorporating the Perdew and Zunger parametrization. The functional is supplemented by the Perdew-Zunger self-interaction correction (SIC) [23]. The SIC corrects the self-interaction errors of LDA and ensures v_{xc} has the accurate $-1/r$ asymptotic behavior. v_{ne} is the ionic potential felt by the valence electrons due to the ionic core and is modeled by the norm-conserving nonlocal Troullier-Martines pseudopotential [24]. v_{las} is the potential describing the external fields of laser in the velocity gauge.

Before propagation in time, the initial states are obtained by solving the KS equations self-consistently at the density functional theory (DFT) level. Then the KS orbitals are propagated

Optics EXPRESS

using the approximate enforced time-reversal symmetry scheme. The time step is 0.05 a.u. and the propagation stops after the laser pulse vanishes. The widths of the simulation box are 64 a.u., 64 a.u., 40 a.u. in the x, y, z directions, respectively. To avoid the reflection of the wavefunction, a sine squared imaginary potential is added at the boundaries. The KS and TDKS equations are discretized and solved with the Octopus package [25–27]. The harmonic spectrum is obtained as

$$S(\omega) = |\int \ddot{\mathbf{D}}(t)\exp(-i\omega t)dt|^2, \tag{3}$$

where the time-dependent dipole is calculated as $\mathbf{D}(t) = \int \mathbf{r}\rho(\mathbf{r},t)d\mathbf{r}$.

3. Results and discussions

In this work, the tartaric acid is chosen as prototype. The tartaric acid molecule is the most common example in textbooks that has two chiral carbons. Three typical stereoisomers of tartaric acid are shown in Fig. 1. The structures of the three stereoisomeric molecules are optimized with the quantum chemistry code Gaussian [28]. Figure 1 also shows the orientations of the molecules, where both chiral carbons are located on the z axis. The orientation of large molecules can be achieved with moderately intense laser pulses [20, 29, 30]. In Fig. 1(a), both chiral carbons of the molecule are R-type. Therefore, this molecule is right-handed chiral and is denoted as RR-tartaric acid. The enantiomer of the RR-tartaric acid is presented in Fig. 1(c), in which both chiral carbons are S-type. This molecule is therefore left-handed chiral and is denoted as SS-tartaric acid. In Fig. 1(b), the upper and lower chiral carbons of the molecule are R-type and S-type respectively. This molecule is a meso isomer and is denoted as RS-tartaric acid. The ionization potentials I_p are 0.324 a.u. for RR- and SS-tartaric acids and 0.295 a.u. for RS-tartaric acid from the DFT calculation.

To investigate the CD of HHG, CP laser pulses with peak intensity $I = 8\times10^{13}$ W/cm^2 and wavelength $\lambda = 800$ nm are applied. The laser pulse propagates in the z direction and polarizes in the $x-y$ plane. In the simulation, the laser pulse has a sine squared envelope with total pulse duration $T = 14$ optical cycles. The vector potentials are therefore written as:

$$A_x(t) = A_0\sin^2(\frac{\pi t}{T})\cos(\omega_0 t), \tag{4}$$

$$A_y(t) = A_0\sin^2(\frac{\pi t}{T})\cos(\omega_0 t \pm \frac{\pi}{2}), \tag{5}$$

where A_0 and ω_0 are the amplitude and angular frequency of the laser field, respectively. The electric fields $\mathbf{E} = -\frac{1}{c}\partial(\mathbf{A})/\partial t$, where c is the speed of light. The electric field of the left CP laser pulse is shown in Fig. 2(a) as an example. Figs. 2(b) and 2(c) show the obtained harmonic spectra from RR- and RS-tartaric acid driven by left and right CP laser pulses, respectively. Based on the semiclassical recollision model, the cutoff position of the harmonic spectrum with CP laser pulses is estimated to be $2U_p + I_p$ [19], where $U_p = E_0^2/4\omega_0^2$ is the ponderomotive energy and E_0 is the amplitude of the electric field [12, 31]. For the applied parameters here, the cutoff position should be around the 9th order, which is consistent with the results in Fig. 2. In Fig. 2(b) both odd and even harmonics are obtained, while only odd harmonics can be found in Fig. 2(c). This is because the selection rule of HHG is determined by the rotational symmetries of the laser field and the projection of the molecule on the polarization plane ($x-y$ plane): If the laser field possesses L-fold rotational symmetry (denoted as C_L) and the projection possesses K-fold rotational symmetry (C_K), the selected harmonic orders are $kJ\pm1$, where $k = 0, 1, 2, \cdots$ and J is the greatest common divisor (GCD) of L and K [32, 33]. Specifically, the projection of the meso isomer possesses C_2 symmetry, while the projections of the chiral isomers possess C_1 symmetry. For the circularly polarized laser pulse, the laser field possesses C_∞ symmetry. Therefore, the selection rule of HHG from the meso isomer is $2k\pm1$, where only odd harmonics

Optics EXPRESS

will be generated. And the selection rule of HHG from the chiral isomers are $k \pm 1$, where both odd and even harmonics are obtained.

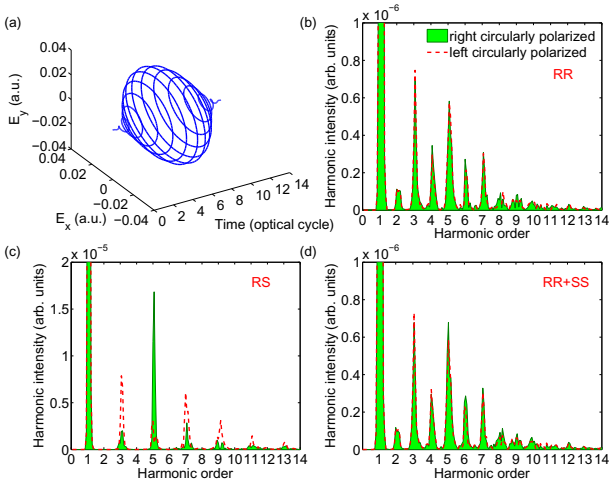

Fig. 2. (a) Electric field of the left CP driving laser pulse. (b) Harmonic spectra from RR-tartaric acid driven by left and right CP laser pulses, respectively. (c) Harmonic spectra from RS-tartaric acid driven by left and right CP laser pulses, respectively. (d) Sum of the high harmonic spectra from RR- and SS-tartaric acids.

The chirality of molecules was discovered because some molecules exhibited optical activity due to their different responses to left and right CP light. A meso isomer is defined as a non-optically active molecule despite containing two or more chiral centers. Therefore, it is commonly known that a chiral molecule exhibits CD while a meso isomer exhibits no CD in conversional optical phenomena. However, from the obtained harmonic spectra shown in Fig. 2, anomalous CD is found. For the RR-tartaric acid, the harmonic spectra driven by left and right CP laser pulses are nearly identical, which means the high harmonic responses of this chiral molecule are the same for CP laser pulses with opposite helicities. The results are the same for SS-tartaric acid that the two harmonic spectra are also nearly identical (not shown). By contrast, the harmonic spectra for RS-tartaric acid driven by left and right CP laser pulses are significantly different.

To quantitatively evaluate the CD of HHG, we calculate [13, 14]

$$|Q| = 2\left|\frac{S_{left}(M) - S_{right}(M)}{S_{left}(M) + S_{right}(M)}\right|, \tag{6}$$

where S_{left} and S_{right} are harmonic yields driven by left and right CP laser pulses respectively. M denotes the harmonic order. The CD can also be evaluated by the ratios of harmonic yields as

$$\beta^2 = \frac{\max[S_{left}(M), S_{right}(M)]}{\min[S_{left}(M), S_{right}(M)]}. \tag{7}$$

We calculate and compare the values of $|Q|$ and β^2 for RR- and RS-tartaric acid as shown in Fig. 3. It is found that, both $|Q|$ and β^2 are very small for the RR-tartaric acid, showing that nearly no CD can be found. On the other hand, $|Q|$ is nearly one order of magnitude higher for RS-tartaric acid than that for RR-tartaric acid, and β^2 is several times higher. From the results, one can see that the different CD signal for the meso isomer and its chiral isomers are significantly distinguishable.

Optics EXPRESS

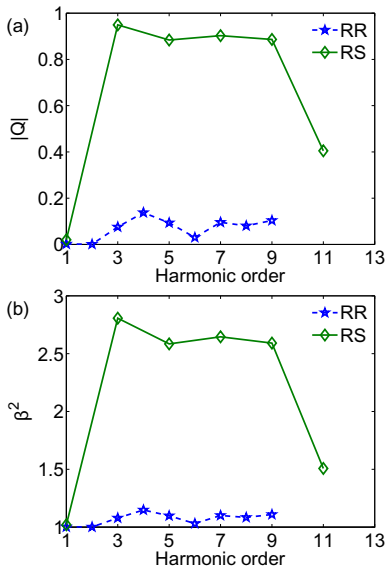

Fig. 3. Values of (a) $|Q|$ and (b) β^2 for the HHG of RR- and RS-tartaric acid.

The next question is why such counterintuitive CD occurs in HHG. To answer the question, we first recall the semiclassical recollision model of HHG [17–19]. According to the recollision model, the HHG process consists of three steps: (i) an electron of the target molecule is ionized to the continuum state, (ii) this liberated electron is accelerated in the laser field, (iii) the electron with particular condition returns to the parent ion and releases the accumulated energy by emitting a harmonic photon. This model can also be described in a quantum mechanical version that the wavepacket is ejected to the continuum state, propagates, and finally recombines to the ground states emitting the high harmonics.

Corresponding to the three-step recollision model, the high harmonic emission can be obtained in the form [34, 35]

$$\mathbf{D} \sim \sum_{\mathcal{P}} a_{ion}[\mathcal{P}]a_{prop}[\mathcal{P}]\mathbf{d}_{rec}[\mathcal{P}], \tag{8}$$

where a_{ion}, a_{prop} and $\mathbf{d}_{rec}$ are the ionization amplitude, propagation amplitude and recombination dipole moment, respectively. According to the path integral formulation of quantum mechanics, the evolution of the wavepacket can be represented by quantum paths. $\mathcal{P}$ denotes the quantum paths contributing to HHG, which are obtained by solving the saddle point equations [36] and can be approximately described by the classical electron trajectories. Since the electrons mainly drift parallel to the $x-y$ plane, the electron trajectories can be divided into two groups: trajectories in the upper half of the molecule (above the $x-y$ plane) and those in the lower half of the molecule (below the $x-y$ plane). Then Eq. (8) is written as

$$\mathbf{D} \sim \sum_{\mathcal{T}\{\text{upper}\}} a_{ion}[\mathcal{T}]a_{prop}[\mathcal{T}]\mathbf{d}_{rec}[\mathcal{T}] \tag{9}$$

$$+ \sum_{\mathcal{T}\{\text{lower}\}} a_{ion}[\mathcal{T}]a_{prop}[\mathcal{T}]\mathbf{d}_{rec}[\mathcal{T}], \tag{10}$$

where $\mathcal{T}$ denotes the electron trajectories. From the recollision model of HHG and Eqs. (8)–(10), it is shown that the electron trajectories play crucial roles in the feature of the high harmonic emission.

Optics EXPRESS

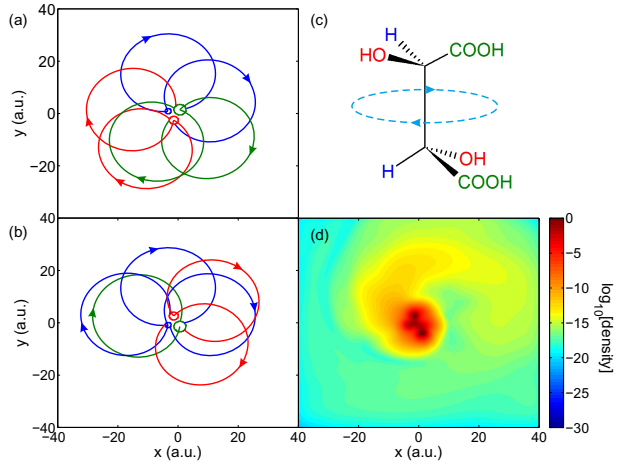

Fig. 4. (a) and (b) Typical electron trajectories for the RR-tartaric acid driven by right CP laser field in the upper and lower halves of the molecule, respectively. The hollow circles represent different ligands and electron trajectories from different ligands are plotted in corresponding colors. (c) For clarify, the configuration of the RR-tartaric acid is presented, with the blue dashed circle indicating the rotation direction of the laser field. (d) Snapshot of density at $t = 9.191$ fs and $z = -2.4$ a.u. in the TDDFT propagation for RR-tartaric acid driven by right CP laser field.

To better understand HHG process of tartaric acids, we calculate the electron trajectories with the classical model [19]. In order to reflect the most essential factors that determine the anomalous CD, we simplify the ligands connected to the chiral carbons (i.e. -H, -OH and -COOH) as spherical entities with different sizes in the classical calculation. The radiuses of the spherical entities are 1 a.u., 1.5 a.u. and 2 a.u. respectively. We consider electrons ionized at different times and from different ligands. The evolution of the ionized electrons is described by the classical equation:

$$\frac{d^2\mathbf{r}}{dt^2} = -\mathbf{E}(t), \tag{11}$$

where $\mathbf{r}$ is the coordinate of the electrons. Several typical electron trajectories for the RR-tartaric acid driven by right CP laser fields are shown in Fig. 4. The electron trajectories are plotted in two groups (in the upper half and the lower half of the molecule) in two-dimensional coordinates. The hollow circles denote the ligands with different sizes and electron trajectories from different ligands are plotted with corresponding colors to increase the readability.

The electron trajectories obtained with this simple classical model depict the major feature of the HHG process: the ionized electrons first travel around the molecule clockwise and then return to the parent ion from different directions (to different ligands one after another). The corresponding quantum mechanical picture of this process is also intuitively shown in Fig. 4(d), where the snapshot of density at $t = 9.191$ fs and $z = -2.4$ a.u. in the TDDFT propagation is presented. It is shown that, the wavepacket is ionized to the continuum state and propagates clockwise around the molecule. During propagation, the continuum wavepacket recombines to the ground state from different directions and the "sees" the different ligands sequentially. In the example shown in Fig. 4, the continuum wavepacket/electrons see the ligands in the order →H→COOH→OH→ in the upper half of the RR-tartaric acid molecule, and see the ligands in the order →H→OH→COOH→ in the lower half. These orders will determine the electron trajectories that contribute to HHG. Note that, as indicated in Eqs. (8)–(10), different electron trajectories lead to different HHG processes and thus different high harmonic emission, while

Optics EXPRESS

same electron trajectories lead to the same high harmonic emission. Therefore, whether the HHG exhibits CD can be determined by the orders of ligands seen by the continuum electrons propagating anticlockwise and clockwise respectively.

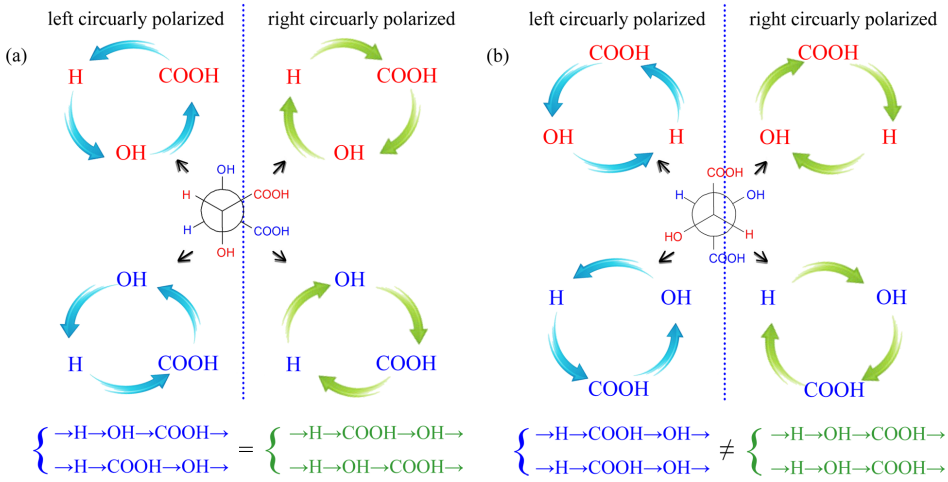

Fig. 5. Analysis for the orders of ligands seen by the continuum electrons for (a) RR-tartaric acid and (b) RS-tartaric acid. The thick arrows indicate the rotation directions of the continuum electrons driven by left (blue) and right (green) CP laser fields respectively. For each molecule, the upper and lower halves are analyzed separately. In panel (a) for RR-tartaric acid, the orders taking account of upper and lower halves are →H→OH→COOH→ + →H→COOH→OH→ for both left and right CP laser pulses. Thus, $\mathcal{T}\{\text{left}\} = \mathcal{T}\{\text{right}\}$ and the obtained spectra are the same in CP laser fields with opposite helicities. In panel (b) for RS-tartaric acid, the orders in both halves are →H→COOH→OH→ for left CP laser pulse and →H→OH→COOH→ for right CP laser pulse. Thus, $\mathcal{T}\{\text{left}\} \neq \mathcal{T}\{\text{right}\}$ and the obtained harmonic spectra in left and right CP laser fields are different.

The orders of ligands seen by the continuum electrons are summarized in Fig. 5. The thick arrows indicate the rotation directions of the continuum electron driven by left (blue) and right (green) CP laser fields, respectively. The upper and lower halves of the molecules are analyzed separately. Figure 5(a) shows the analysis for RR-tartaric acid. The continuum electrons rotate anticlockwise in left CP laser field and see the ligands in the order →H→OH→COOH→ in the upper half of the RR-tartaric acid (top-left corner of Fig. 5(a)). In the same laser field, the continuum electrons see the ligands in the order →H→COOH→OH→ in the lower half (bottom-left corner of Fig. 5(a)). Driven by the right CP laser field, the order is →H→COOH→OH→ in the upper half (top-right corner of Fig. 5(a)) and is →H→OH→COOH→ in the lower half (bottom-right corner of Fig. 5(a)). Based on the above analysis of the orders, it is found that the trajectories in the upper half with left CP laser field are the same as the those in the lower half with right CP laser field, i.e.

$$\mathcal{T}\{\text{upper, left}\} = \mathcal{T}\{\text{lower, right}\}. \tag{12}$$

In the same way,

$$\mathcal{T}\{\text{lower, left}\} = \mathcal{T}\{\text{upper, right}\}. \tag{13}$$

Therefore, for the HHG process of the whole RR-tartaric acid molecule, the trajectories with left and right CP laser fields are the same:

$$\mathcal{T}\{\text{left}\} = \mathcal{T}\{\text{right}\}. \tag{14}$$

Optics EXPRESS

Thus, the obtained harmonic spectra from the RR-tartaric acid driven by CP laser fields with opposite helicities should be the same, as is shown in Fig. 2(b).

For the RS-tartaric acid shown in Fig. 5(b), the orders are →H→COOH→OH→ for both the upper and lower halves driven by the left CP laser field. To the contrary, the orders are →H→OH→COOH→ for both the upper and lower halves driven by the right CP laser field. As a result, for the HHG process of the whole RS-tartaric acid molecule

$$\mathcal{T}\{\text{left}\} \neq \mathcal{T}\{\text{right}\}, \tag{15}$$

and the obtained high harmonic emissions driven by left and right CP laser fields are different. This also agrees with the results shown in Fig. 2(c). From the above discussion, it can be concluded that the anomalous CD found in HHG is essentially due to the characteristic strong-field recollision dynamics of HHG.

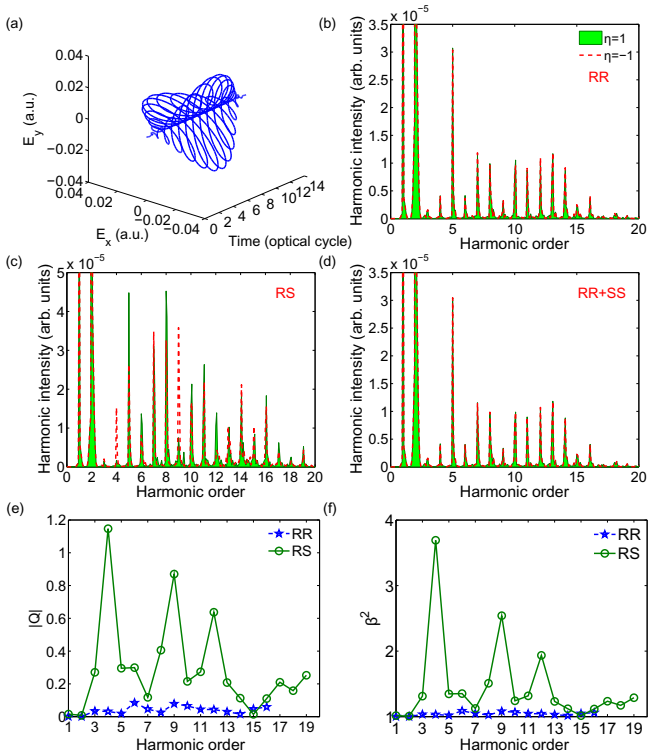

Fig. 6. (a) Electric field of the CRB pulse with $\eta = 1$. (b) Harmonic spectra from RR-tartaric acid driven by CRB laser pulses with $\eta = -1$ and 1, respectively. (c) Harmonic spectra from RS-tartaric acid driven by CRB laser pulses with $\eta = -1$ and 1, respectively. (d) Sum of the high harmonic spectra from RR- and SS-tartaric acids. (e) Values of $|Q|$ for RR- and RS-tartaric acid. (f) Values of β^2 for RR- and RS-tartaric acid.

This anomalous CD in HHG promises the opportunity to discriminate the meso isomer and racemic mixture. Since the high harmonic emissions with left and right CP laser pulses are the same for both the right-handed and left-handed chiral isomers, the detected harmonic spectra from a racemic mixture driven by CP laser pulses with opposite helicities should also be the same. As a demonstration, the sum of the high harmonic spectra of RR- and SS-tartaric acids is presented in Fig. 2(d). It is shown that, the harmonic spectra with different CP laser pulses are nearly the same. Therefore, by comparing the different CD of the obtained high harmonic signal, the meso and racemic samples can be discriminated.

Optics EXPRESS

Apart from CP laser pulses, the chirality can also be detected with CRB laser pulses. A CRB laser field is composed of two coplanar counter-rotating CP laser fields with different frequencies [16, 37–39]. By using the CRB laser pulses, the efficiency of HHG can be dramatically increased with the chiral dichroism signal still high [14]. Next, we will discuss on the dichroism response of HHG from the tartaric acid molecules driven by CRB laser pulses. In our calculation, the applied CRB laser pulse is composed of the 1000 nm and 500 nm CP laser pulses. The peak intensities of the two CP laser pulses are 2×10^{13} W/cm^2, and both pulses have sine squared envelope with total pulse duration $T = 14$ optical cycles of the 1000 nm pulse. The vector potentials are in the form:

$$A_x(t) = \sin^2(\frac{\pi t}{T})[A_{01}\sin(\omega_0' t) + A_{02}\sin(2\omega_0' t)], \tag{16}$$

$$A_y(t) = \eta\sin^2(\frac{\pi t}{T})[A_{01}\cos(\omega_0' t) - A_{02}\cos(2\omega_0' t)], \tag{17}$$

where $\eta = \pm1$. A_{01} and A_{02} are the peak amplitudes of vector potentials for the 1000 nm and 500 nm laser pulses. ω_0' is the frequency of the 1000 nm laser field. The laser fields rotate in opposite directions for $\eta = -1$ and 1 respectively. The electric field of the CRB pulse with $\eta = 1$ is shown in Fig. 6(a) as an example.

The obtained harmonic spectra of RR- and RS-tartaric acid are shown in Figs. 6(b) and 6(c). Compared with the harmonic spectra obtained with CP laser pulses, the high harmonic signals obtained with CRB laser pulses are one order of magnitude higher and consequently the signal-to-noise-ratio will be improved. Besides, since the CRB laser field possesses C_3 symmetry, the selection rules for both meso and chiral isomers are $k \pm 1$, where odd and even harmonics are obtained in the harmonic spectra [32, 33]. Comparing the results with $\eta = -1$ and 1, it is found that the harmonic spectra are nearly the same for RR-tartaric acid and are significantly different for RS-tartaric acid. The harmonic spectra of SS-tartaric acid are also nearly the same with $\eta = -1$ and 1 (not shown). Fig. 6(d) shows the harmonic spectra by summing the spectra of RR- and SS-tartaric acids. It is shown that the results with $\eta = -1$ and 1 are nearly the same. This dichroism phenomenon can be explained in the same way as that for CP driving laser pulses, because the continuum electrons also rotate around the molecules before recombination and thus the high harmonic emission is dependent on the orders of ligands seen by the continuum electrons. The dichroism response can also be quantitatively evaluated by calculating $|Q|$ and β^2. The results for RR- and RS-tartaric acid are shown in Figs. 6(e) and (f). From the values of $|Q|$ and β^2, it is shown that the dichroism signals for the RR-tartaric acid are about one order of magnitude higher than those for RS-tartaric acid at most harmonic orders. These results indicate that the meso and racemic samples can also be discriminated by applying the CRB laser pulses instead of CP laser pulses.

4. Conclusion

In summary, the HHG of three different stereoisomeric tartaric acid molecules are studied. Since the tartaric acid contains two chiral centers, the three stereoisomers are right-handed chiral molecule, meso isomer and left-handed chiral molecule respectively. It is found that, driven by CP laser fields with opposite helicities, the harmonic spectra are nearly the same for the chiral isomers while the spectra are significantly different for the meso isomer. This anomalous CD phenomenon is explained based on the semiclassical recollision model of HHG. It is shown that, whether the obtained harmonic spectra are the same is determined by the orders of ligands (-H, -OH, -COOH) seen by the continuum electrons. This feature makes the HHG a promising tool to discriminate the meso isomer and racemic mixture. We also investigate the HHG of tartaric acid driven by CRB laser pulses and similar dichroism responses are found, which implies the meso and racemic samples can be discriminated by alternatively applying the CRB laser

Optics EXPRESS

pulses. Recently, the HHG in solid samples has attracted more and more attentions [40, 41]. The mechanism of HHG in solid is still in discussion. Therefore, it will be a very interesting question to see whether the anomalous circular dichroism of HHG can be found in solid samples, like crystalized tartaric acid, for future investigation.

Funding

National Natural Science Foundation of China (NSFC) (11404123, 11234004, 61275126, 11422435, 11574101).

Acknowledgments

Numerical simulations presented in this paper were carried out using the High Performance Computing Center experimental testbed in SCTS/CGCL (see http://grid.hust.edu.cn/hpcc).